Molecular Basis of Phosphatidylinositol 4-Phosphate and ARF1 GTPase Recognition by the FAPP1 Pleckstrin Homology (PH) Domain*[S]

Ju He[‡], Jordan L. Scott[§], Annie Heroux[¶], Siddhartha Roy[‡], Marc Lenoir[‖], Michael Overduin[‖], Robert V. Stahelin[§**1], and Tatiana G. Kutateladze[‡2]

From the [‡]Department of Pharmacology, University of Colorado School of Medicine, Aurora, Colorado 80045, the [§]Department of Chemistry and Biochemistry and the Walther Center for Cancer Research, University of Notre Dame, Notre Dame, Indiana 46556, the [**]Department of Biochemistry and Molecular Biology, Indiana University School of Medicine, South Bend, Indiana 46617, the [¶]Department of Biology, Brookhaven National Laboratory, Upton, New York 11973, and the [‖]School of Cancer Sciences, University of Birmingham, Birmingham B15 2TT, United Kingdom

Four-phosphate-adaptor protein 1 (FAPP1) regulates secretory transport from the trans-Golgi network (TGN) to the plasma membrane. FAPP1 is recruited to the Golgi through binding of its pleckstrin homology (PH) domain to phosphatidylinositol 4-phosphate (PtdIns(4)P) and a small GTPase ADP-ribosylation factor 1 (ARF1). Despite the critical role of FAPP1 in membrane trafficking, the molecular basis of its dual function remains unclear. Here, we report a 1.9 Å resolution crystal structure of the FAPP1 PH domain and detail the molecular mechanisms of the PtdIns(4)P and ARF1 recognition. The FAPP1 PH domain folds into a seven-stranded β-barrel capped by an α-helix at one edge, whereas the opposite edge is flanked by three loops and the β4 and β7 strands that form a lipid-binding pocket within the β-barrel. The ARF1-binding site is located on the outer side of the β-barrel as determined by NMR resonance perturbation analysis, mutagenesis, and measurements of binding affinities. The two binding sites have little overlap, allowing FAPP1 PH to associate with both ligands simultaneously and independently. Binding to PtdIns(4)P is enhanced in an acidic environment and is required for membrane penetration and tubulation activity of FAPP1, whereas the GTP-bound conformation of the GTPase is necessary for the interaction with ARF1. Together, these findings provide structural and biochemical insight into the multivalent membrane anchoring by the PH domain that may augment affinity and selectivity of FAPP1 toward the TGN membranes enriched in both PtdIns(4)P and GTP-bound ARF1.

Four-phosphate-adaptor protein 1 (FAPP1)[3] controls the formation and fission of post-Golgi vesicles and regulates secretory transport from the trans-Golgi network (TGN) to the plasma membrane (1). Displacement or knockdown of FAPP1 inhibits the cargo transfer, whereas FAPP1 overexpression impairs carrier fission (1, 2). Recruitment of FAPP1 to the TGN membranes, particularly to the exit sites where transport carriers are formed, requires association of its pleckstrin homology (PH) domain with phosphatidylinositol 4-phosphate (PtdIns(4)P), a primary phosphoinositide (PI) lipid in the Golgi complex, and with a small GTPase ARF1 (ADP-ribosylation factor 1) (1). Despite the vital role of FAPP1 in membrane budding and trafficking, the molecular mechanisms by which this protein exerts its functions remain unclear.

Human FAPP1 is a 300-residue protein that contains an N-terminal PH domain followed by a short proline-rich motif (see Fig. 1). The FAPP1 PH domain represents a distinct subset of PH modules capable of interacting with two ligands in contrast to a typical PH domain that has a single binding partner. Approximately 20% of PH domain-containing proteins have been found to recognize PIs, with PtdIns(4,5)P_2 and PtdIns(3,4,5)P_3 being the most common targets (3–5). Several PH domains, including those of phospholipase C$_{β2}$, phospholipase C$_{γ2}$, and ARHGAP21, are involved in protein-protein interactions and association with Rac1, Rac2, and ARF1 GTPases, respectively, but these PH domains do not bind PIs (6–9). More recently, the PH domains of FAPP1, GRP1, and oxysterol-binding protein were shown to recognize both PI lipids and ARF proteins (1, 10–13); however, the structural and biochemical basis of this dual recognition has not been determined.

ARF1 belongs to the Ras family of small GTPases that control various fundamental signaling processes (14–16). ARF1 regu-

[3] The abbreviations used are: FAPP1, four-phosphate-adaptor protein 1; PI, phosphoinositide; PtdIns, phosphatidylinositol; PtdIns(4)P, phosphatidylinositol 4-phosphate; Ins(1,4)P_2, inositol 1,4-bisphosphate; PH, pleckstrin homology; ARF1, ADP-ribosylation factor 1; TGN, trans-Golgi network; SPR, surface plasmon resonance; HSQC, heteronuclear single quantum coherence; TROSY, transverse relaxation optimized spectroscopy; POPC, 1-palmitoyl-2-oleoyl-sn-glycero-3-phosphocholine; POPE, 1-palmitoyl-2-oleoyl-sn-glycero-3-phosphoethanolamine; PI4P, phosphatidylinositol 4-phosphate.

lates the assembly and disassembly of the vesicle coat machinery at TGN and is involved in the reorganization of actin cytoskeleton and activation of lipid-modifying enzymes (14, 17). Like other GTPases, ARF1 functions as a molecular switch by way of cycling between the inactive GDP-bound state and the active GTP-bound state. The GDP-to-GTP exchange and subsequent ARF1 activation are mediated by guanine nucleotide exchange factors, whereas ARF1 inactivation and GTP hydrolysis are catalyzed by ARF-GAP1 (GTPase-activating protein 1). Human ARF1 is composed of 181 residues folded into an amphipathic α-helix followed by a catalytic guanine nucleotide-binding module (18). ARF1 is myristoylated at the N termini, and this modification is essential for localization to membranes. It has recently been shown that activated ARF1 recruits PI4-kinase III β to the Golgi membrane, elevating the local concentration of PtdIns(4)P and stimulating the rapid accumulation of FAPP1 (1). On the other hand, the ARF1 level in the TGN membranes can be increased by overexpression of FAPP1 PH that may inhibit activity of ARF-GAP1 and protect PtdIns(4)P from degradation (1). Clearly the cross-talk between ARF1, FAPP1 PH, and PtdIns(4)P, the key components of the TGN membrane budding machinery, plays an important role, yet how these components are assembled is unknown.

The mechanism of the dual anchoring to membranes is central for understanding the role of FAPP1 in mediating secretory transport. In this study, we elucidate the molecular basis of PtdIns(4)P and ARF1 recognition using a combination of x-ray crystallographic and NMR analyses, measurements of binding affinities, mutagenesis, and monolayer penetration. and membrane tubulation assays. Our findings provide insight into the mechanistic details of the FAPP1-PtdIns(4)P-ARF1 assembly, demonstrating that the two interactions can occur simultaneously and independently.

EXPERIMENTAL PROCEDURES

Materials—1-Palmitoyl-2-oleoyl-*sn*-glycero-3-phosphocholine (POPC) and 1-palmitoyl-2-oleoyl-*sn*-glycero-3-phosphoethanolamine (POPE) were purchased from Avanti Polar Lipids. Dibutanoyl (C_4)-PtdIns(4)P and Ins(1,4)P_2 were from Echelon, and dipalmitoyl (C_{16})-PtdIns(4)P was from Cayman Chemical Company. $^{15}NH_4Cl$ and $^{13}C_6$-glucose were purchased from Isotech. DL-Seleno-methionine, CHAPS, and thrombin were from Sigma. TALON resin and glutathione-Sepharose columns were from Clontech Laboratories and Amersham Biosciences, respectively.

Subcloning, Expression, and Purification of FAPP1 PH, ARF1, and ARF1 Q71L—DNA fragments encoding residues 1–99, 1–115, 1–121, 1–125, 1–138, and 1–180 of human FAPP1 were cloned into a pET-28a vector (Invitrogen) using NcoI/XhoI restriction sites. A thrombin cleavage site was engineered between the C terminus of FAPP1 and a His$_6$ tag. The 1–99 construct of the Fapp1 PH domain carrying C94S mutation was chosen for biochemical and structural analysis. For simplicity, in this study we refer to the C94S mutant as the FAPP1 PH domain. The unlabeled, ^{15}N-labeled, ^{15}N/^{13}C-labeled, and Se-Met-labeled proteins were expressed in *Escherichia coli* Rosetta (DE3) pLysS in LB or minimal media supplemented with $^{15}NH_4Cl$, $^{13}C_6$-glucose, and DL-seleno-methionine. Bacteria

were harvested by centrifugation after induction with isopropyl-1-thio-β-D-galactopyranoside (0.1 mM) at room temperature for 6 h. The cells were lysed by sonication in lysis buffer (50 mM HEPES, pH 7.6, 300 mM NaCl, 5 mM β-mercaptoethanol, 10% glycerol, and a protease inhibitor mixture). The His$_6$ fusion proteins were purified on a TALON resin column. The His tag was cleaved with thrombin. The proteins were further purified by size exclusion chromatography on a Superdex™ 75 column in either Bis-Tris or HEPES and concentrated in Millipore concentrators. The same protocol was used for expression and purification of K7A, R18A, and K45A mutants of FAPP1 PH. The E50A, H54A, and I64E mutants of glutathione *S*-transferase (GST)-FAPP1 PH were expressed in *E. coli* BL21(DE3) cells and purified as described (19).

The full-length wild type human ARF1 cloned in pGEX-3X vector (a gift from R. Prekeris) and constitutively active mouse ARF1 Q71L lacking the N-terminal residues 1–17 (hereafter called ARF1 Q71L) cloned in pProEX HT vector (a gift from S. Wakatsuki) were expressed and purified as described above. The unlabeled and ^{15}N-labeled proteins were expressed in *E. coli* BL21(DE3) cells in LB or minimal media supplemented with $^{15}NH_4Cl$. The GST fusion wild type human ARF1 was purified on a glutathione-Sepharose column. The His$_6$ tag fusion mouse ARF1 Q71L was purified on a TALON resin column. The GST and His tags were cleaved with factor Xa and tobacco etch virus protease (Invitrogen), respectively. The ARF1 proteins were further purified by FPLC on a Superdex™ 75 column and concentrated in Millipore concentrators.

X-ray Crystallography—The crystals of FAPP1 PH domain were obtained at 18 °C using a hanging drop vapor diffusion method and the precipitant solution containing 0.1 M NaAc, pH 4.6, 50 mM (NH$_4$)$_2$SO$_4$, and 15% PEG 1000. The crystals were soaked in mother liquor supplemented with 20% glycerol and flash-frozen in liquid nitrogen. The x-ray crystallographic data were collected at the National Synchrotron Light Source (NSLS) at the Brookhaven National Laboratory. Data were processed with D*TREK (20). The structure was determined using the Se-Met single anomalous dispersion method and the program hkl2map. The initial models were built using COOT (21) and refined with the program Phenix (22). Statistics are shown in supplemental Table 1.

PCR Mutagenesis—Site-directed mutagenesis of the FAPP1 PH domain was performed using a QuikChange kit (Stratagene). The sequences of the C94S, K7A, K7E, R18A, R18L, K45A, E50A, H54A, and I64E constructs of FAPP1 PH were confirmed by DNA sequencing.

NMR Spectroscopy and Sequence-specific Assignments—Multidimensional heteronuclear NMR spectra were recorded at 25 °C on a Varian INOVA 600-MHz spectrometer. The amino acid sequential assignments of the ^{15}N/^{13}C-labeled FAPP1 PH domain were obtained by collecting and analyzing a set of triple-resonance experiments, including HNCACB, CBCA(CO)NH, HNCO, C(CO)NH, and H(CCO)NH as described in Ref. 23. Spectra were processed with NMRPipe (24) and analyzed using CCPN (25), nmrDraw, and in-house software programs.

NMR Titrations of PtdIns(4)P, Ins(1,4)P$_2$, ARF1, and ARF1 Q71L—The ^{1}H,^{15}N heteronuclear single quantum coherence (HSQC) spectra of 0.1–0.5 mM ^{15}N-labeled FAPP1 PH domain were recorded on Varian INOVA 500-, 600-, and 900-MHz spectrometers. Lipid and Ins(1,4)P$_2$ binding was characterized by monitoring chemical shift changes in the ^{1}H,^{15}N HSQC spectra of the FAPP1 PH domain as 20 mM C$_4$-PtdIns(4)P or Ins(1,4)P$_2$ was added stepwise. The normalized chemical shift changes were calculated using the equation $[(\Delta\delta_H)^2 + (\Delta\delta_N/5)^2]^{0.5}$, where $\Delta\delta_H$ and $\Delta\delta_N$ are ^{1}H and ^{15}N chemical shift changes in parts per million (ppm). Significant changes in the resonances were judged to be greater than the average plus 0.65 S.D. for the titration of C$_4$-PtdIns(4)P.

The NMR titration of unlabeled ARF1 Q71L into the ^{15}N-labeled FAPP1 PH domain (in the presence and absence of PtdIns(4)P) and the reverse titration of unlabeled FAPP1 PH into ^{15}N-labeled ARF1 Q71L were carried out on a Varian INOVA 900-MHz spectrometer. Transverse relaxation optimized spectroscopy (TROSY) spectra of the ^{15}N-labeled protein (0.15 mM) were recorded as the unlabeled ligand-protein was gradually added to a 1:10 ratio. Significant changes in the resonances were judged to be greater than the average plus 0.6 (no lipid) and 0.7 (with the lipid) S.D.

Protein-Lipid Overlay—Protein-lipid overlay assays were performed as described in Ref. 26 using PIP-Strip membranes (Echelon, Inc.) spotted with 100 pmol of various lipids. Membranes were preblocked with 3% BSA in buffer (10 mM Tris-HCl, pH 7.4, 150 mM NaCl, and 0.1% Tween 20), incubated with GST fusion FAPP1 PH at 4 °C for 2 h, and washed five times with buffer. The bound protein was detected by chemiluminescence using anti-GST monoclonal antibodies and an anti-mouse horseradish peroxidase conjugate.

SPR Measurements—The surface plasmon resonance (SPR) experiments were carried out at 25 °C in 10 mM HEPES, pH 7.4 or 10 mM KH$_2$PO$_4$, pH 6.5 buffers containing 160 mM KCl as described in Refs. 19 and 27. POPC/POPE/PI4P (75:20:5) and POPC/POPE (80:20) vesicles were spread onto the active and control surfaces until a response of 5000 resonance units was achieved. Equilibrium SPR measurements were performed at a flow rate of 3 μl/min, providing sufficient time to reach the equilibrium response (R_{eq}). Sensorgrams were obtained using seven or more different concentrations of proteins (within a 10-fold range of K_d values) and corrected for the refractive index change by subtracting the control surface response. After plotting R_{eq} *versus* the total protein concentration (P$_0$), the K_d value was determined by a nonlinear least-squares analysis of binding isotherms using the equation: $R_{eq} = R_{max}/(1 + K_d/P_0)$ (28).

Protein-protein interactions were investigated using a CM5 chip. ARF1 or ARF1 Q71L was amine-coupled to the CM5 chip by injecting the protein (50 ng/ml) at the rate of 5 μl/min over flow channel 2. Flow channel 1 was used as a control and subjected to the amine-coupling reagents, but no protein was added. FAPP1 PH was injected at a rate of 10 μl/min into both flow channels. Equilibrium SPR analysis was done as described above. The k_{off} for the interaction of FAPP1 PH with ARF1 was analyzed by fitting the dissociation phase of the binding curves

and determining the $t_{1/2}$ of each dissociation phase ($k_{off} = 0.69302/t_{1/2}$).

Membrane Tubulation Assays—Glass coverslips (22 × 40 mm) were cleaned by sonication in 1% 7X (MP Biomedicals). After vigorous rinses and sonication in distilled water to remove any trace of detergent, coverslips were washed with 100% ethanol and dried under N$_2$. To generate membrane sheets, 1 μl of lipid solution (POPC/POPE (80:20) or POPC/POPE/PI4P (75:20:5)) in chloroform (10 mg/ml) was spotted on each coverslip and dried under N$_2$ for 30 min to remove traces of chloroform. Lipids were prehydrated for 20–30 min in a small chamber and then fully rehydrated by adding 15–20 μl of buffer (10 mM HEPES, pH 7.4, 160 mM KCl, 10 mM FM 2-10). With the chamber mounted on a Zeiss LSM710 microscope stage, 1 μl of protein solution (2.5 mg/ml) was injected into the chamber. The deformation of membrane sheets into vesicles and tubules was monitored using laser excitation at 488 nm and recording emission above 510 nm. The formation of the narrow tubules was monitored by differential interference contrast microscopy as described in Ref. 29.

Liposome Pelleting Assays—Liposome assays were carried out as described previously (19). Briefly, FAPP1 PH (0, 1, 2, 5, and 10 μM) and DOPC/DOPE (80:20) or DOPC/DOPE/PI4P (80:18:2) liposomes were incubated for 15 min at room temperature in a 20 mM Tris buffer, 100 mM NaCl, 2 mM DTT. The pellets were collected by centrifugation at 100,000 × g for 15 min at 4 °C. The pelleted fraction and supernatant were examined by SDS-PAGE gel electrophoresis using Coomassie Blue staining. The amount of the bound protein was determined using an Ingenus light box and the GeneTools software (Syngene).

Monolayer Measurements—The insertion of FAPP1 PH into a phospholipid monolayer was investigated by measuring the change in surface pressure (π) of the invariable surface area upon the addition of the protein (23, 30). POPC/POPE (80:20) or POPC/POPE/PI4P (75:20:5) monolayers were spread onto the subphase composed of 10 mM HEPES, 160 mM KCl (pH 7.4) until the desired initial surface pressure (π_0) was reached. After stabilization of the signal (~5 min), 10 μg of FAPP1 PH was injected into the subphase. The surface pressure change $\Delta\pi$ was monitored for 45 min.

GST Pulldown—10 μg of His-ARF1 Q71L was incubated with 40 μg of wild type or mutated GST-FAPP1 PH at 4 °C for 2 h in binding buffer (10 mM HEPES, pH 7.4, 150 mM NaCl, 1 mM DTT) prior to the addition of 10 μl of glutathione-Sepharose beads. The bead fraction was collected by centrifugation and washed three times. His-ARF1 Q71L, precipitated with GST-FAPP1 bound to the beads, was detected by Western blotting using anti-His antibodies. The experiments were performed in triplicate.

RESULTS AND DISCUSSION

Overall Structure of the FAPP1 PH Domain—To elucidate the molecular basis of the PtdIns(4)P and ARF1 recognition, we obtained the three-dimensional structure of the human FAPP1 PH domain (residues 1–99, C94S mutant, hereafter called FAPP1 PH). The structure was determined at a 1.9 Å resolution by x-ray crystallography (Fig. 1). The PH domain crystallized as
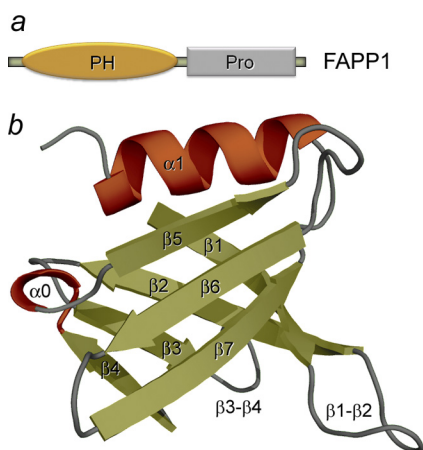
FIGURE 1. **The crystal structure of the PH domain of FAPP1 (C94S) determined at 1.9 Å resolution.** *a*, architecture of FAPP1: the amino-terminal PH domain and a proline-rich motif. *b*, ribbon diagram of the FAPP1 PH structure.

a dimer of two identical molecules linked through a C-terminal extension. The single FAPP1 PH domain folds into a seven-stranded β-barrel capped by an α-helix at one edge. The opposite edge of the β-barrel is flanked by the β4 and β7 strands and three loops: a long β1-β2 loop, a β3-β4 loop that is partially invisible in the structure, and a short β6-β7 loop. An additional one-turn α-helix is formed between the β4 and β5 strands. The crystal structure of the FAPP1 PH domain and the solution structure of this protein (Protein Data Bank (PDB) 2KCJ) (31) superimposed with a root mean square deviation of 2.1 Å over Cα atoms, with the differences seen in the position of the β5-β6 loop and the β4 and β7 strands that comprise the lipid-binding site (see below). The secondary structure elements in FAPP1 PH aligned well with that of a canonical PH module, such as human GRP1 PH (PDB 1FGZ) (32) (root mean square deviation of 1.9 Å over all Cα atoms and root mean square deviation of 1.1 Å over Cα atoms in β-strands/α-helix), indicating that the overall fold of the β-barrel and the main α-helix is conserved within the PH domain family. The diffraction data and refinement statistics for the crystal structure are shown in supplemental Table 1.

PtdIns(4)P-binding Site—To define the mechanism of lipid binding, we investigated the association of the FAPP1 PH domain with PtdIns(4)P by NMR, SPR, and mutagenesis (Fig. 2). The ^{1}H,^{15}N HSQC spectra of uniformly ^{15}N-labeled protein were collected while a water-soluble dibutanoyl (C$_4$) form of PtdIns(4)P was titrated in the NMR sample (Fig. 2*a*). As C$_4$-PtdIns(4)P was added stepwise, a number of the FAPP1 PH amide resonances underwent changes indicating a direct interaction between the protein and the lipid, which was in agreement with the previous reports (1, 26, 31). Similar in directions but smaller in magnitude chemical shift changes in the PH domain spectra were induced by Ins(1,4)P$_2$, an isolated head group of PtdIns(4)P (Fig. 2, *a* and *b*). These results suggested that both ligands occupy the same binding pocket with the inositol ring being involved in the most significant contacts; however, the presence of the diacylglycerol moiety of the lipid is essential for strong interaction. We note that the fast exchange regime on the NMR time scale indicated that even the short chain C$_4$-PtdIns(4)P form was bound weakly, in the low mM
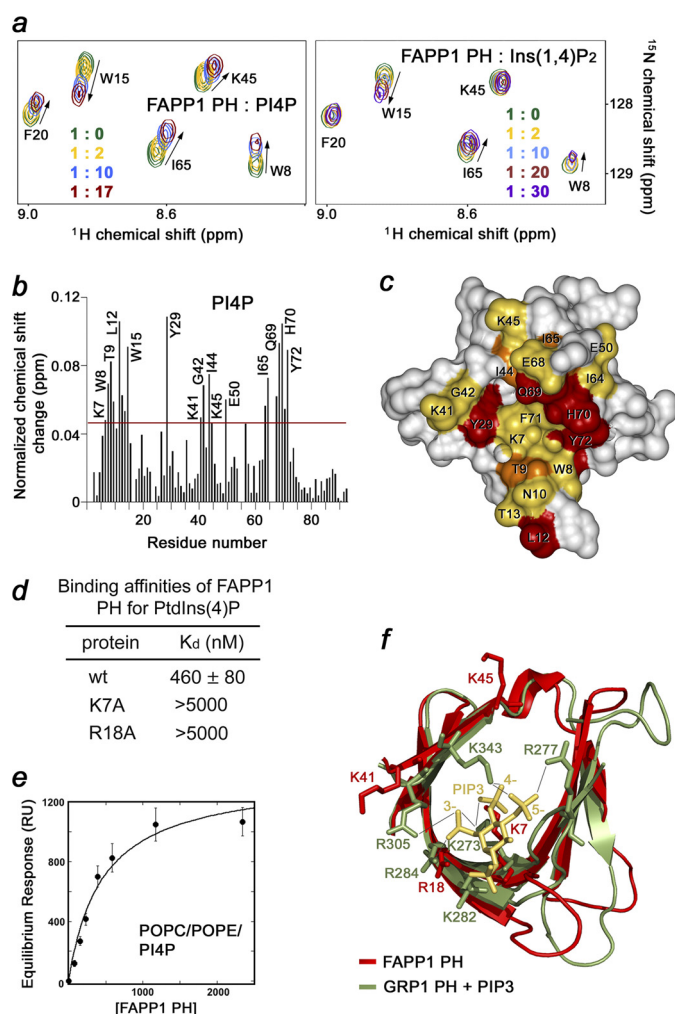

FIGURE 2. **The PtdIns(4)P-binding site of the FAPP1 PH domain.** *a*, superimposed ^{1}H,^{15}N HSQC spectra of ^{15}N-labeled FAPP1 PH collected during titration with C$_4$-PtdIns(4)P (PI4P) or the lipid head group, Ins(1,4)P$_2$. The spectra are color-coded according to the concentration of the ligands. *b*, the histogram shows normalized chemical shift changes induced in the backbone amides of the PH domain by PtdIns(4)P. *c*, residues that display significant chemical shift change in *b* are labeled on the FAPP1 PH domain surface and colored *red*, *orange*, and *yellow* for large, medium, and small changes, respectively. *d*, binding affinities of the wild type and mutant FAPP1 PH domain for POPC/POPE/PI4P (75:20:5) vesicles were measured by SPR. *e*, representative binding isotherms generated from saturation response values at respective FAPP1 PH concentrations were used to calculate K_d. *RU*, resonance units. *Error bars* indicate S.D. *f*, overlay of the β-barrels of the FAPP1 PH domain (*red*) and the PtdIns(3,4,5)P$_3$-bound GRP1 PH domain (1FGY). PtdIns(3,4,5)P$_3$ is shown as a *stick model* and colored *yellow*. Selected hydrogen bonds in the GRP1 complex are depicted as *gray lines*.

range. The binding became considerably stronger when a long chain dipalmitoyl (C$_{16}$)-PtdIns(4)P form embedded in POPC/POPE vesicles was used. The dissociation constant (K_d) for the interaction with C$_{16}$-PtdIns(4)P, measured by SPR, was found to be 460 ± 80 nM (Fig. 2, *d* and *e*).

The PtdIns(4)P-binding site was mapped based on chemical shift changes observed in FAPP1 PH upon binding of C$_4$-PtdIns(4)P (Fig. 2*b*). The largest resonance perturbations occurred in the β4 and β7 strands and the β1-β2 loop of the protein, suggesting that the open edge of the β-barrel comprises the binding site for the lipid. Compared with resonance perturbations previously reported for binding of the C$_6$-form of the lipid (31), C$_4$-PtdIns(4)P induced larger changes in the

$\beta1$-$\beta2$ loop but smaller changes in the $\beta4$ strand. Mapping the changes onto the PH domain surface revealed a well defined, deep pocket in the interior of the barrel where PtdIns(4)P is bound (Fig. 2*c*). A high positive potential of the pocket suggested that electrostatic and hydrogen-bonding interactions play an essential role in the recognition of the lipid head group.

The side chains of the basic amino acids Lys-7, Arg-18, Lys-41, and Lys-45 are well positioned to coordinate the negatively charged phosphate groups of the inositol ring. These residues clearly overlay with the basic residues of the GRP1 PH domain that make major contacts with PtdIns(3,4,5)P$_3$ (32, 33) (Fig. 2*f*). Particularly, residues Lys-273 and Lys-343 form hydrogen bonds to the 4-phosphate group in the GRP1 PH-PtdIns(3,4,5)P$_3$ complex (32, 33), and the similarly positioned Lys-7 and Lys-45 of the FAPP1 PH domain may coordinate the 4-phosphate group of PtdIns(4)P. To assess the importance of the basic residues in the PtdIns(4)P-binding pocket, we generated the K7A and R18A mutants and tested them by SPR. The data shown in Fig. 2*d* and supplemental Fig. 1 demonstrate that substitution of Lys-7 or Arg-18 abrogates interaction of the FAPP1 PH domain with C$_{16}$-PtdIns(4)P-containing vesicles, underscoring the critical role of the basic residues in lipid binding.

Interactions with PtdIns(4)P Is pH-dependent—To gain mechanistic insight, we analyzed specificity and examined factors that may influence binding of FAPP1. The specificity of the FAPP1 PH domain was tested by a protein-lipid overlay assay. Nitrocellulose membranes were spotted with 100 pmol of PIs and other lipids and incubated with GST-FAPP1 PH. The membrane-bound protein was detected by Western blot analysis using anti-GST antibodies. As shown in Fig. 3*a*, GST-FAPP1 PH recognized PtdIns(4)P but did not bind other lipids, corroborating the finding of the Alessi group (26). Superimposition of the FAPP1 and GRP1 PH domains provides a possible explanation of the preference for PtdIns(4)P (Fig. 2*f*). The FAPP1 PH domain lacks the basic residue necessary for coordination of the 5-phosphate group in the GRP1 PH-PtdIns(3,4,5)P$_3$ complex (Arg-277) and therefore cannot accommodate the trisphosphorylated PI. The fact that Arg-18 and Lys-41 of the FAPP1 PH domain are positioned in the same way as the 3-phosphate-coordinating Arg-284 and Arg-305 residues of GRP1 suggests that the FAPP1 PH domain could bind bisphosphorylated species, which is also supported by previous observations (31).

The FAPP1 PH-PtdIns(4)P interaction was facilitated by lowering the pH of the medium. We performed ^{1}H,^{15}N HSQC titration experiments at pH 6.5 and 7.4 (Fig. 3*b*). Whereas at pH 7.4, C$_4$-PtdIns(4)P caused small chemical shift changes in the FAPP1 PH domain, substantially larger changes were seen at pH 6.5, implying that binding was stronger under the acidic conditions. The binding affinities measured by SPR revealed that the FAPP1 PH domain binds POPC/POPE/C$_{16}$-PtdIns(4)P vesicles with a K_d of 200 $\pm$ 10 nM at pH 6.5; however, it associates 2.3-fold weaker at pH 7.4 (Fig. 3*c* and supplemental Fig. 2). The pH dependence is most likely due to the presence of a histidine residue in the binding site, *i.e.* His-70 in the $\beta7$ strand that undergoes protonation in an acidic environment, increasing a positive net charge of the binding pocket. Alignment of the
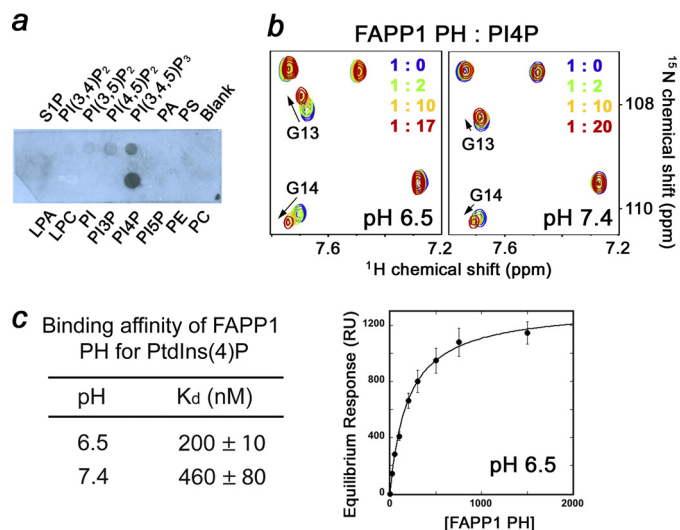

FIGURE 3. **PtdIns(4)P binding is pH-sensitive.** *a*, the specificity of FAPP1 PH was assessed by a protein-lipid overlay assay. *S1P*, sphingosine 1-phosphate; *PI(3,4)P$_2$*, phosphatidylinositol 3,4-bisphosphate; *PI(3,5)P$_2$*, phosphatidylinositol 3,5-bisphosphate; *PI(4,5)P$_2$*, phosphatidylinositol 4,5-bisphosphate; *PI(3,4,5)P$_3$*, phosphatidylinositol 3,4,5-trisphosphate; *PA*, phosphatidic acid; *PS*, phosphatidylserine; *LPA*, lysophosphatidic acid; *LPC*, lysophosphatidylcholine; *PI3P*, phosphatidylinositol 3-phosphate; *PI5P*, phosphatidylinositol 5-phosphate; *PE*, phosphatidylethanolamine; *PC*, phosphatidylcholine. *b*, superimposed ^{1}H,^{15}N HSQC spectra of ^{15}N-labeled FAPP1 PH collected during the gradual addition of C$_4$-PtdIns(4)P at pH 6.5 and 7.4. *c*, binding affinities of the wild type FAPP1 PH domain for POPC/POPE/PI4P (75:20:5) vesicles as measured by SPR. Representative binding isotherm at pH 6.5 was used to calculate K_d values. *RU*, resonance units. *Error bars* indicate S.D.

amino acid sequences of several PH domains reveals that this histidine residue is conserved in a set of proteins, including GRP1 (supplemental Fig. 3). The corresponding His-355 of GRP1 forms a hydrogen bond with the 4-phosphate group of PtdIns(3,4,5)P$_3$ (32, 33) and mediates pH sensitivity (23).

It is well established that FAPP1 localizes exclusively to the TGN membranes where intravesicular pH is 6.4. However, it does not localize to the plasma membrane at the cytosolic pH of 7.4, despite the fact that the plasma membrane contains a small pool of PtdIns(4)P. Furthermore, translocation of cytosolic Arf1 to membranes depends on intravesicular acidification (34). Although further studies are required to determine whether the FAPP1 PH domain can sense the pH gradient across the Golgi membrane, it has recently been shown that another PI-binding module, the FYVE domain, displays similar pH-dependent intracellular distribution (19, 35). It associates with PtdIns(3)P-enriched membranes of early endosomes, which have a low pH lumen, but not with other PtdIns(3)P-containing membranes. Additionally, protonation/deprotonation of the His residue in the PI-binding site can modulate affinity of the FAPP1 PH domain as cytosolic pH fluctuations occur (36–39). Taken together, our data indicate that the direct interaction of the FAPP1 PH domain with PtdIns(4)P is pH-dependent; it is weak at the cytosolic pH of 7.4 but becomes stronger at pH 6.5.

PtdIns(4)P Binding of the FAPP1 PH Domain Is Required for the Membrane Insertion and Tubulation—It has recently been shown that the $\beta1$-$\beta2$ loop of FAPP1 PH inserts into membrane-mimicking micelles causing deformation of the lipid layer (31). To determine whether PtdIns(4)P binding is neces-
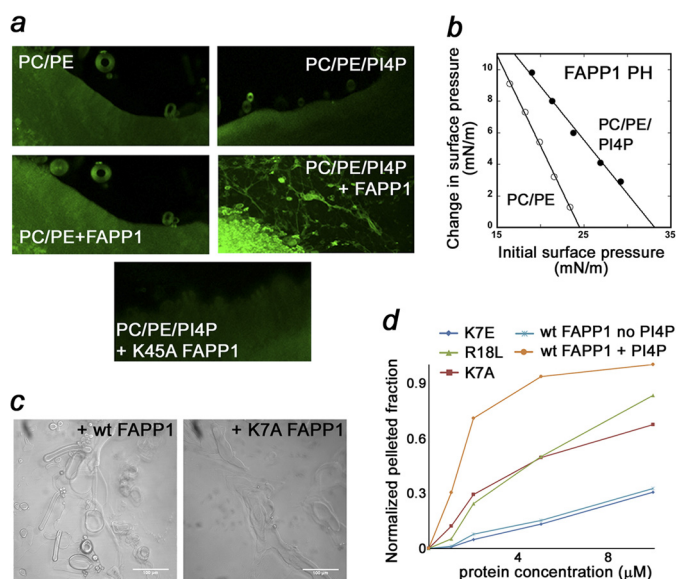
FIGURE 4. **Binding of the FAPP1 PH domain to PtdIns(4)P is necessary for membrane tubulation, pelleting, and insertion.** *a, top panels*, POPC/POPE (80:20) and POPC/POPE/PI4P (75:20:5) membrane sheets labeled with FM 2-10 dye. *Middle panels*, 2.5 mg/ml FAPP1 PH was injected. Images are shown after 5 min (*left*) and 2 min (*right*) of incubation with FAPP1 PH. (*bottom panel*) POPC/POPE/PI4P membrane sheets after 5 min of incubation with 2.5 mg/ml K45A FAPP1 PH. *PC*, phosphatidylcholine; *PE*, phosphatidylethanolamine. *b*, the insertion of the FAPP1 PH domain into a POPC/POPE (80:20) monolayer (*open circles*) and a POPC/POPE/PtdIns(4)P (75:20:5) monolayer (*filled circles*). *c*, the formation of narrow membrane tubules caused by WT or mutated FAPP1 PH was examined by differential interference contrast microscopy. *d*, graphs showing normalized pelleted fraction of WT and mutant FAPP1 PH plotted as a function of the initial protein concentration.

FIGURE 5. **The ARF1-binding site of the FAPP1 PH domain.** *a*, superimposed ^1H,^{15}N TROSY spectra of ^{15}N-labeled FAPP1 PH collected as unlabeled ARF1 Q71L was titrated in. The spectra are color-coded according to the concentration of ARF1 Q71L. *b*, the histogram shows normalized chemical shift changes induced in the backbone amides of the PH domain by ARF1 Q71L. *c*, residues that display significant chemical shift change in *b* are labeled on the ribbon diagram of FAPP1 PH and colored *red* and *pink* for large and medium changes, respectively. *d*, superimposed ^1H,^{15}N TROSY spectra of ^{15}N-labeled ARF1 Q71L recorded while unlabeled FAPP1 PH was added stepwise.

sary for the FAPP1 function, the wild type protein and the K7A, K7E, R18L, and K45A mutants impaired in PtdIns(4)P binding were examined in membrane tubulation, pelleting, and monolayer penetration assays (Fig. 4). POPC/POPE (80:20) or POPC/POPE/PI4P (75:20:5) membrane sheets were treated with the lipophilic dye FM 2-10 to obtain high resolution imaging by a confocal microscope. Whereas the addition of the FAPP1 PH domain to POPC/POPE sheets did not cause detectable changes in the morphology of the membrane sheets up to 10 min, the addition of the protein to PtdIns(4)P-containing membrane sheets rapidly induced tubulation (Fig. 4*a*). In contrast, when K45A mutant of FAPP1 PH defective in PtdIns(4)P binding was incubated with PtdIns(4)P-containing membrane sheets, the membrane deformation was abrogated completely. The K7A, K7E, and R18L mutants of FAPP1 PH were also unable to induce the formation of narrow tubules, and the pelleting function of these mutants was significantly compromised (Fig. 4, *c* and *d*). We concluded that interaction with PtdIns(4)P is critical for FAPP1 to induce membrane deformation.

Likewise the insertion of the FAPP1 PH domain into POPC/POPE monolayers required the presence of PtdIns(4)P (Fig. 4*b*). The FAPP1 PH domain exhibited low intrinsic membrane-penetrating ability. The POPC/POPE (80:20) monolayer surface pressure (π_c) was found to be ~24 millinewtons/m; however, incorporation of 5 mol % PtdIns(4)P into the lipid monolayer greatly enhanced penetration, raising the π_c value to ~33 millinewtons/m. These results underscored the essential role of the PtdIns(4)P recognition for biological activities of FAPP1 PH.
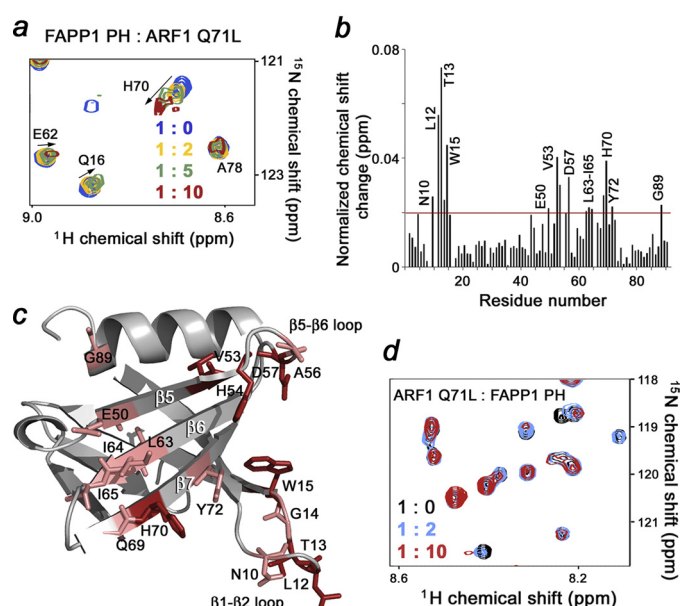
ARF1-binding Site of the FAPP1 PH Domain—To understand how ARF1 is recognized by the FAPP1 PH domain, the ARF1-binding site of FAPP1 PH was identified by NMR, SPR, mutagenesis, and pulldown assays. ^1H,^{15}N TROSY spectra of ^{15}N-labeled FAPP1 PH were recorded as the unlabeled constitutively active GTP-locked ARF1 Q71L mutant lacking the N-terminal residues 1–17 (ARF1 Q71L) was added stepwise to a 1:10 ratio (Fig. 5*a*). Chemical shift perturbations and disappearance of the signals upon the addition of ARF1 Q71L pointed to a direct interaction between the two proteins. The most pronounced chemical shift changes were observed for residues located in the long β1-β2 loop (Asn-10, Leu-12, Thr-13, Gly-14, and Trp-15), the β5-β6 loop (Ala-56 and Asp-57), the β5, β6, and β7 strands (Glu-50, Val-53, His-54, Leu-63, Ile-64, Ile-65, Gln-69, His-70, and Tyr-72), and the far C terminus of the α-helix (Gly-89) (Fig. 5*b*), indicating that these residues are directly or indirectly involved in the interaction. Mapping these residues on the structure of the FAPP1 PH domain outlined an extended site that spreads across the β5-β7 sheet of the β-barrel and is flanked by the β1-β2 and β5-β6 loops (Fig. 5*c*).

The direct interaction between ARF1 Q71L and the FAPP1 PH domain was substantiated by a reverse titration of unlabeled FAPP1 PH into the ^{15}N-labeled ARF1 Q71L protein (Fig. 5*d*). As in the experiments described above, a number of amide cross-peaks in ^1H,^{15}N TROSY spectra of ARF1 Q71L decreased in intensity and changed their positions upon the addition of FAPP1 PH, indicating binding.

To define the role of the most perturbed residues of the FAPP1 PH domain, the E50A, H54A, and I64E mutants were generated and tested by pulldown assays. His-tagged ARF1 Q71L was first incubated with the wild type or mutated GST-
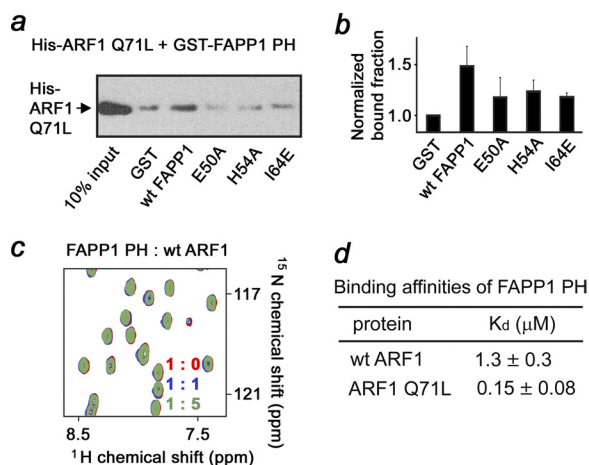
FIGURE 6. **The GTP-bound conformation of ARF1 is essential.** *a* and *b*, mutations of the ARF1-binding site residues disrupt binding. Pulldown assays and the histogram show that His-ARF1 Q71L is precipitated by wild type or mutant GST-FAPP1 PH bound to the glutathione-Sepharose beads. *Error bars* indicate S.D. *c*, superimposed ^{1}H,^{15}N TROSY spectra of ^{15}N-labeled FAPP1 PH collected as wild type ARF1 was titrated in. *d*, binding affinities of the FAPP1 PH domain for ARF1 as measured by SPR. Kinetic curves were used to calculate K_d and k_{off}.

FAPP1 PH domain and then with glutathione-Sepharose beads. After collecting the beads by centrifugation, bound ARF1 Q71L was detected by Western blot using antibodies against the His tag. As shown in Fig. 6, *a* and *b*, wild type GST-FAPP1 PH precipitated ARF1 Q71L, whereas the E50A, H54A, and I64E mutants of FAPP1 PH lost their ability to associate with ARF1 Q71L. Thus, the FAPP1 residues located in the β5 and β6 strands are necessary for the interaction.

The GTP-bound Form of ARF1 Is Essential—Because binding of GTP activates ARF1, we next examined whether the ARF1 conformation plays a role in association with FAPP1 PH. A lack of significant changes in ^{1}H,^{15}N TROSY spectra of the ^{15}N-labeled FAPP1 PH domain upon the addition of unlabeled wild type ARF1 indicated that the GTP-free form of ARF1 does not associate with FAPP1 PH (Fig. 6c). To quantitatively characterize the effect of GTP, we measured binding affinity of the FAPP1 PH domain for wild type ARF1 and GTP-locked ARF1 Q71L by SPR. As shown in Fig. 6d, FAPP1 PH binds ARF1 Q71L ~9-fold more strongly than it binds wild type ARF1. Furthermore, the off-rate for the interaction with wild type ARF1 was ~10-fold faster as compared with the off-rate for the interaction with ARF1 Q71L. These data demonstrate that the GTP-bound form of ARF1 is required for the strong interaction with FAPP1 PH.

FAPP1 Can Bind PtdIns(4)P Lipid and ARF1 Simultaneously and Independently—We explored a cross-talk between the two ligands using NMR and SPR analyses (Fig. 7). The head group of the lipid, Ins(1,4)P$_2$, was titrated into the FAPP1 PH domain alone or FAPP1 PH prebound to ARF1 Q71L (Fig. 7b). Almost identical in the magnitude and directions chemical shift changes were observed in both NMR experiments, indicating that the head group of PtdIns(4)P was bound similarly and the formation of the FAPP1-ARF1 Q71L complex did not affect lipid binding. In agreement, when ARF1 Q71L was gradually added to the ligand-free FAPP1 PH domain or FAPP1 PH prebound to PtdIns(4)P, a similar pattern of resonance perturba-
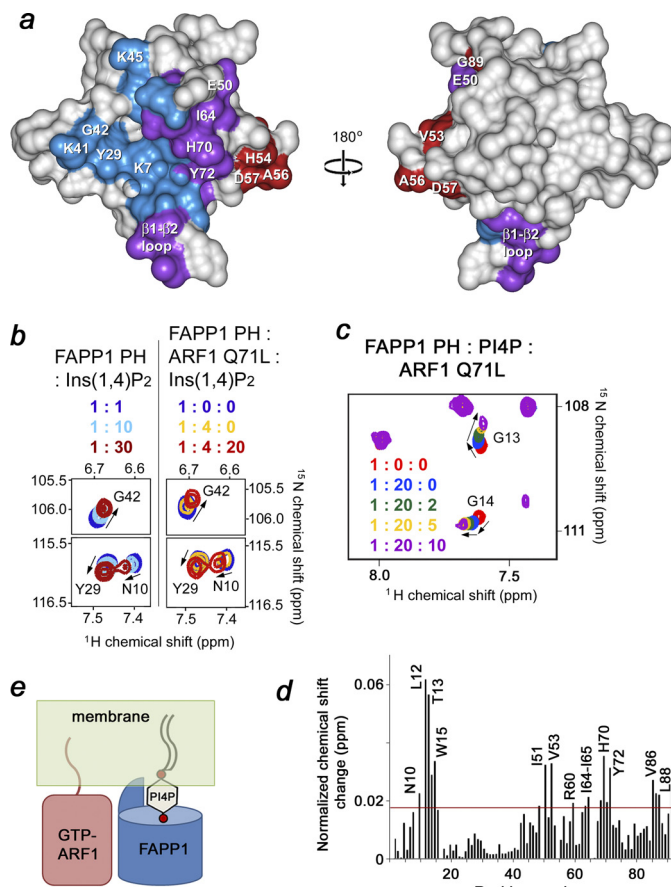

FIGURE 7. **Molecular mechanism of PtdIns(4)P and ARF1 recognition.** *a*, the residues of FAPP1 PH most perturbed upon interaction with either PtdIns(4)P, ARF1 Q71L, or both ligands are mapped on the surface of the PH domain and colored *blue*, *red*, and *purple*, respectively. *b*, superimposed ^{1}H,^{15}N HSQC spectra of FAPP1 PH (*left*) and ^{1}H,^{15}N TROSY spectra of FAPP1 PH prebound to ARF1 Q71L collected during titration with Ins(1,4)P$_2$. *c*, superimposed ^{1}H,^{15}N TROSY spectra of FAPP1 PH recorded as first C$_4$-PtdIns(4)P and then ARF1 Q71L were titrated in. *d*, the histogram shows normalized chemical shift changes induced in the backbone amides of the C$_4$-PtdIns(4)P-bound FAPP1 PH domain by ARF1 Q71L. *e*, a model of anchoring of FAPP1 PH to the Golgi membranes via the double interaction with PtdIns(4)P lipid and myristoylated GTP-bound ARF1.

tions was seen (Figs. 5b and 7d). These results suggested that the ARF1 Q71L-binding site and the strength of the FAPP1 PH-ARF1 interaction were not altered by PtdIns(4)P binding. Furthermore, the K7A mutant of FAPP1 impaired in lipid binding associated with ARF1 Q71L as strong as the wild type FAPP1 PH domain and exhibited comparable dissociation kinetics. Although the PtdIns(4)P- and ARF1-binding sites are located in close proximity and residues in the β5-β7 sheet and the β1-β2 loop were perturbed upon binding of either ligand, the sites have little overlap as the lipid-binding pocket is positioned within the β-barrel, whereas the ARF1-binding site is located on the external side of the β-barrel (Fig. 7e). Together, our findings suggest that FAPP1 PH is able to bind PtdIns(4)P and ARF1 simultaneously and independently.

In conclusion, in this study we detail the molecular mechanism of the dual recognition of PtdIns(4)P and ARF1 by the FAPP1 PH domain and demonstrate that the two ligands can associate with the PH domain independently. Our results indicate that the PtdIns(4)P- and ARF1-binding sites are located on

the internal and external sides of the β-barrel and that binding to PtdIns(4)P is enhanced in an acidic environment, whereas interaction with ARF1 requires the GTP-bound conformation of the GTPase. The binary association of the FAPP1 PH domain may increase binding affinity and selectivity toward the TGN membranes enriched in both PtdIns(4)P lipid and GTP-bound ARF1 anchored to membranes through a myristoyl moiety x (Fig. 7*e*).

REFERENCES

1. Godi, A., Di Campli, A., Konstantakopoulos, A., Di Tullio, G., Alessi, D. R., Kular, G. S., Daniele, T., Marra, P., Lucocq, J. M., and De Matteis, M. A. (2004) *Nat. Cell Biol.* **6,** 393–404
2. D'Angelo, G., Vicinanza, M., Di Campli, A., and De Matteis, M. A. (2008) *J. Cell Sci.* **121,** 1955–1963
3. DiNitto, J. P., and Lambright, D. G. (2006) *Biochim Biophys Acta* **1761,** 850–867
4. Lemmon, M. A. (2008) *Nat. Rev. Mol. Cell Biol.* **9,** 99–111
5. Kutateladze, T. G. (2010) *Nat. Chem. Biol.* **6,** 507–513
6. Jezyk, M. R., Snyder, J. T., Gershberg, S., Worthylake, D. K., Harden, T. K., and Sondek, J. (2006) *Nat. Struct. Mol. Biol.* **13,** 1135–1140
7. Ménétrey, J., Perderiset, M., Cicolari, J., Dubois, T., Elkhatib, N., El Khadali, F., Franco, M., Chavrier, P., and Houdusse, A. (2007) *EMBO J.* **26,** 1953–1962
8. Bunney, T. D., Opaleye, O., Roe, S. M., Vatter, P., Baxendale, R. W., Walliser, C., Everett, K. L., Josephs, M. B., Christow, C., Rodrigues-Lima, F., Gierschik, P., Pearl, L. H., and Katan, M. (2009) *Mol. Cell* **34,** 223–233
9. Snyder, J. T., Singer, A. U., Wing, M. R., Harden, T. K., and Sondek, J. (2003) *J. Biol. Chem.* **278,** 21099–21104
10. Levine, T. P., and Munro, S. (2002) *Curr. Biol.* **12,** 695–704
11. Cohen, L. A., Honda, A., Varnai, P., Brown, F. D., Balla, T., and Donaldson, J. G. (2007) *Mol. Biol. Cell* **18,** 2244–2253
12. Lemmon, M. A. (2004) *Biochemical Society transactions* **32,** 707–711
13. Balla, A., Tuymetova, G., Tsiomenko, A., Várnai, P., and Balla, T. (2005) *Mol. Biol. Cell* **16,** 1282–1295
14. D'Souza-Schorey, C., and Chavrier, P. (2006) *Nat. Rev. Mol. Cell Biol.* **7,** 347–358
15. Kahn, R. A., Cherfils, J., Elias, M., Lovering, R. C., Munro, S., and Schurmann, A. (2006) *J. Cell Biol.* **172,** 645–650
16. Gillingham, A. K., and Munro, S. (2007) *Annu. Rev. Cell Dev. Biol.* **23,** 579–611
17. Donaldson, J. G. (2008) *Biochem. J.* **414,** e1–2
18. Liu, Y., Kahn, R. A., and Prestegard, J. H. (2009) *Structure* **17,** 79–87
19. He, J., Vora, M., Haney, R. M., Filonov, G. S., Musselman, C. A., Burd, C. G., Kutateladze, A. G., Verkhusha, V. V., Stahelin, R. V., and Kutateladze, T. G. (2009) *Proteins* **76,** 852–860
20. Pflugrath, J. W. (1999) *Acta Crystallogr. D Biol. Crystallogr.* **55,** 1718–1725
21. Emsley, P., and Cowtan, K. (2004) *Acta Crystallogr. D Biol. Crystallogr.* **60,** 2126–2132
22. Adams, P. D., Grosse-Kunstleve, R. W., Hung, L. W., Ioerger, T. R., McCoy, A. J., Moriarty, N. W., Read, R. J., Sacchettini, J. C., Sauter, N. K., and Terwilliger, T. C. (2002) *Acta Crystallogr. D Biol. Crystallogr.* **58,** 1948–1954
23. He, J., Haney, R. M., Vora, M., Verkhusha, V. V., Stahelin, R. V., and Kutateladze, T. G. (2008) *J. Lipid Res.* **49,** 1807–1815
24. Delaglio, F., Grzesiek, S., Vuister, G. W., Zhu, G., Pfeifer, J., and Bax, A. (1995) *J. Biomol. NMR* **6,** 277–293
25. Vranken, W. F., Boucher, W., Stevens, T. J., Fogh, R. H., Pajon, A., Llinas, M., Ulrich, E. L., Markley, J. L., Ionides, J., and Laue, E. D. (2005) *Proteins* **59,** 687–696
26. Dowler, S., Currie, R. A., Campbell, D. G., Deak, M., Kular, G., Downes, C. P., and Alessi, D. R. (2000) *Biochemical J.* **351,** 19–31
27. Hom, R. A., Vora, M., Regner, M., Subach, O. M., Cho, W., Verkhusha, V. V., Stahelin, R. V., and Kutateladze, T. G. (2007) *J. Mol. Biol.* **373,** 412–423
28. Cho, W., Bittova, L., and Stahelin, R. V. (2001) *Anal. Biochem.* **296,** 153–161
29. Cao, X., Coskun, U., Rössle, M., Buschhorn, S. B., Grzybek, M., Dafforn, T. R., Lenoir, M., Overduin, M., and Simons, K. (2009) *Proc. Natl. Acad. Sci. U.S.A.* **106,** 21121–21125
30. Lee, S. A., Kovacs, J., Stahelin, R. V., Cheever, M. L., Overduin, M., Setty, T. G., Burd, C. G., Cho, W., and Kutateladze, T. G. (2006) *J. Biol. Chem.* **281,** 37091–37101
31. Lenoir, M., Coskun, U., Grzybek, M., Cao, X., Buschhorn, S. B., James, J., Simons, K., and Overduin, M. (2010) *EMBO Rep* **11,** 279–284
32. Lietzke, S. E., Bose, S., Cronin, T., Klarlund, J., Chawla, A., Czech, M. P., and Lambright, D. G. (2000) *Mol. Cell* **6,** 385–394
33. Ferguson, K. M., Kavran, J. M., Sankaran, V. G., Fournier, E., Isakoff, S. J., Skolnik, E. Y., and Lemmon, M. A. (2000) *Mol. Cell* **6,** 373–384
34. Zeuzem, S., Feick, P., Zimmermann, P., Haase, W., Kahn, R. A., and Schulz, I. (1992) *Proc. Natl. Acad. Sci. U.S.A.* **89,** 6619–6623
35. Lee, S. A., Eyeson, R., Cheever, M. L., Geng, J., Verkhusha, V. V., Burd, C., Overduin, M., and Kutateladze, T. G. (2005) *Proc. Natl. Acad. Sci. U.S.A.* **102,** 13052–13057
36. Gottlieb, R. A., Giesing, H. A., Zhu, J. Y., Engler, R. L., and Babior, B. M. (1995) *Proc. Natl. Acad. Sci. U.S.A.* **92,** 5965–5968
37. Moolenaar, W. H., Tsien, R. Y., van der Saag, P. T., and de Laat, S. W. (1983) *Nature* **304,** 645–648
38. Schuldiner, S., and Rozengurt, E. (1982) *Proc. Natl. Acad. Sci. U.S.A.* **79,** 7778–7782
39. Thangaraju, M., Sharma, K., Leber, B., Andrews, D. W., Shen, S. H., and Srikant, C. B. (1999) *J. Biol. Chem.* **274,** 29549–29557